HiSST: 3rd International Conference on
High-Speed Vehicle Science Technology
14 -19 April 2024, Busan, Korea

Compressible correction and correlation of γ-Re_θ transition model for high-speed flows

Yuxiang Fan[1], Rui Zhao[2,3], Xu Zhang[4]

Abstract

Based on the original γ-Re_θ transition model framework, in this work, an improved local correlation-based transition closure model is developed for high-speed flows. The local correlation between the vorticity Reynolds number and the momentum thickness Reynolds number obtained by compressible boundary-layer self-similar solutions, local compressibility correction including the pressure gradient parameter and momentum thickness Reynolds number, and local crossflow correlation are applied to improve the original γ-Re_θ model for hypersonic transition predictions. The function F_{onset1} used to control the transition onset as well as several relevant model parameters are also modified to make the improved model suitable for high-speed flow. The improved transition model is validated through several basic test cases under a wide range of flow conditions, including high-speed flat plates, sharp cones, HIFiRE-5, and complex hypersonic configuration X-33 vehicles. The numerical results show that the transition onset locations and the changes of heat transfer rate predicted by the present improved transition model are reasonably consistent with experimental results. The proposed model predicts the high-speed boundary layer transition behaviors induced by streamwise and crossflow instabilities with reasonable precision.

Keywords: High-speed, γ-Re_θ transition model, Local compressible correction, Local correlation, Boundary layer transition

1. Introduction

Boundary layer transition is the process from a laminar to a turbulent flow. For hypersonic vehicles, boundary layer transition directly affects factors including wall drag, aerodynamic heating, and propulsive efficiency. Thus, the accurate prediction of transitional flows is important in the design of hypersonic vehicles. However, because of strong complexity, nonlinearity, and various impact factors, boundary layer transitions are hard to predict precisely.

In recent decades, a variety of approaches have been proposed for predicting transitions, including stability-based analyses with the e^N method, transition models, large eddy simulations (LES), and direct numerical simulations (DNS). Reynolds-averaged Navier-Stokes (RANS)-based transition models have attracted much interest in the research community owing to their flexible compatibility with modern computational fluid dynamics (CFD) methods, reasonable prediction accuracy, and low computational costs compared with the LES and DNS approaches. The use of massively parallel computing and unstructured meshes forms the mainstream of modern engineering CFD applications, so it is sensible to try to avoid solving non-local variables. In order to meet these requirements and incorporate different transition paths, Menter et al.[1] and Langtry et al.[2] proposed the concept of local correlation-based transition modeling (LCTM). Their first model was the well-known γ-Re_θ transition model [3].

[1] *Beijing Institute of Technology, 5 Zhongguancun South Street, Haidian District, Beijing, China, ffanyuxaing@163.com*
[2] *Beijing Institute of Technology, 5 Zhongguancun South Street, Haidian District, Beijing, China, zr@bit.edu.com*
[3] Chongqing Innovation Center, Beijing Institute of Technology, *Tongmao Avenue, Yubei District, Chongqing, China, zr@bit.edu.cn*
[4] *Beijing Institute of Technology, 5 Zhongguancun South Street, Haidian District, Beijing, China, zx_9199@163.com*

Therefore, this paper focuses on using the γ-Re_θ correlation based on the LCTM framework to predict high-speed flow transitions, considering a greater number of relevant factors for high-speed flows.

2. Transition Model Descriptions

2.1. Local correlation between Re_v and Re_θ

In Eq.(1), the function F_{onset1} is mainly used to control the transition onset and is defined as follows:

$$F_{\text{onset1}} = \frac{Re_v}{2.193 Re_{\theta c}} \tag{1}$$

The correlation in Eq. (1), based on the observation of a Blasius boundary layer, was first proposed by Wilcox [4] . The application of the correlation can allow for the avoidance of additional nonlocal boundary layer parameters in transition predictions. However, the original numerical relationship for low-speed flows is unsuitable for high-speed flows, so we need a new proportional relationship to replace the original equation and obtain the appropriate relationship for high-speed boundary layers. Inspired by the work of Liu et al. [5,6], the compressible boundary layer self-similar solution is used to obtain the local correlation between Re_v and Re_θ. To better fit the framework of the γ-Re_θ transition model, we omit the pressure gradient part of the original paper here and modify the pressure gradient using another method, which will be explained later. The influence of the pressure gradient on the correlation was studied in Ref. 7, and it was found that the relative error is not of great concern under general conditions when the new correlation obtained by fitting similarity solutions with a zero pressure gradient is used in transition models. Therefore, the final calculation formula we use is as follows, and more specific content can be found in the original paper [6]. Since this function (1) mainly controls the streamwise transition, in order to better describe and distinguish it from the local crossflow transition onset function in the following, we define a new variable $F_{\text{onset,s}}$:

$$F_{\text{onset,s}} = \frac{Re_v}{F_{\text{ratio}}\left(Ma_{eL}, T_{eL}, T_w\right) Re_{\theta c}} \tag{2}$$

$$\left(\frac{Re_{v,\max}}{Re_\theta}\right)_L = F_{\text{ratio}}\left(Ma_{eL}, T_{eL}, T_w\right) = \left[a_1\left(\frac{T_{eL}}{T_w}\right)^{a_2} + a_3\right] \tag{3}$$

$$\begin{aligned} a_1 &= 1.882\cdot10^{-4} Ma_{eL}^3 + 4.544\cdot10^{-3} Ma_{eL}^2 - 1.954\cdot10^{-1} Ma_{eL} + 1.748 \\ a_2 &= 1.667\cdot10^{-4} Ma_{eL}^3 - 2.171\cdot10^{-3} Ma_{eL}^2 - 2.937\cdot10^{-2} Ma_{eL} - 0.5902 \\ a_3 &= -8.928\cdot10^{-4} Ma_{eL}^3 + 2.041\cdot10^{-2} Ma_{eL}^2 + 9.166\cdot10^{-2} Ma_{eL} + 0.4975 \end{aligned} \tag{4}$$

Ma_{eL} and T_{eL} are local variables calculated using the engineering method proposed by Xu et al. [8] and Qiao et al.[9], and are used to determine the non-local variables Ma_e and T_e, as this approach performs well in high-speed transitional flow simulations. Ma_{eL} and T_{eL} are estimated using the following equations:

$$\begin{aligned} &\left(\frac{r_g}{r_g-1}\right)\frac{P_\infty}{\rho_\infty} + \frac{U_\infty^2}{2} = \left(\frac{r_g}{r_g-1}\right)\frac{P}{\rho_{eL}} + \frac{U_{eL}^2}{2} \\ &\rho_{eL} = \rho_\infty\left(\frac{P}{P_\infty}\right)^{1/r_g} \\ &\frac{a_\infty^2}{r_g-1} + \frac{U_\infty^2}{2} = \frac{a_{eL}^2}{r_g-1} + \frac{U_{eL}^2}{2} \\ &Ma_{eL} = \frac{U_{eL}}{a_{eL}} \\ &T_{eL} = \frac{a_{eL}^2}{r_g R} \end{aligned} \quad , \tag{5}$$

where R is the gas constant and r_g is the gas-specific heat capacity ratio. Therefore, the calculation process is transformed strictly into local variables.

2.2. Local compressibility correction

In the original transition model, the calculation of $Re_{\theta t}$ contains information on the pressure gradient, but the calculation is based on a low-speed incompressible flow. With an increase in the Mach number, the characteristics of the boundary layer become different, and the original correlation is unsuitable for high-speed flows. Based on the theory of a compressible boundary layer, by analyzing the relationships between the pressure gradient parameter and the Mach number, the following correction is obtained:

$$\lambda_{\theta,\text{new}} = \lambda_\theta \left(1 + \frac{r_g - 1}{2} Ma_{eL}^2\right), \tag{6}$$

where λ_θ is the original pressure gradient parameter and Ma_{eL} is the local variable calculated using the engineering method, which determines the non-local Ma_e Mach number at the outer edge of the boundary layer.

The critical momentum thickness Reynolds number correlation $Re_{\theta c}$ in the original transition model based on the low-speed experimental case is purely empirical and does not consider the effect of compressibility. It is observed in experiments that the Reynolds number at transition onset changes due to compressibility at high Mach numbers compared with that in incompressible experimental data [10]. By analyzing the boundary-layer variables calculated using the grid-reordering method for massively parallel execution [11] and comparing with the results of Ref. 10, we reformulate and propose a new compressible correction relation for high-speed flows. To better fit the indirect transition prediction in the γ-Re_θ transition model, that is, the progression from $Re_{\theta t}$ to $\tilde{R}e_{\theta t}$ to $Re_{\theta c}$, we add the compressibility correction to the calculation of $Re_{\theta t}$. The compressibility correction is not explicitly applied to the trigger judgment of Eq. (1), but is realized by modifying $Re_{\theta t}$. This has the advantage of not affecting the value of $Re_{\theta c}$ obtained by the convection and diffusion of $\tilde{R}e_{\theta t}$ in the boundary layer. The changes required for the compressibility modification from the original transition model are proposed as:

$$Re_{\theta t,\text{new}} = \frac{Re_{\theta t}}{f(Ma_{eL})} \tag{7}$$

$$f(Ma_{eL}) = -83.16 Ma_{eL}^{-4.095} + 1.509\,, \tag{8}$$

where $Re_{\theta t}$ is the original transition onset momentum-thickness Reynolds number. For numerical robustness, $f(Ma_{eL})$ is bounded as follows:

$$f(Ma_{eL}) = \max(f(Ma_{eL}), 0.1) \tag{9}$$

2.3. Local crossflow-induced correlation

In the present model, the crossflow correlation is based on the concept of local helicity. The crossflow transition correlation follows the method suggested by Ref.5. Local helicity has been widely used as a crossflow indicator in local correlation-based models. The local crossflow transition onset function is given by

$$F_{\text{onset,cf}} = \frac{\Delta H_{\text{cf}} Re_v}{F_{\text{ratio}}(Ma_{eL}, T_{eL}, T_w) C_{\text{cf}}}, \tag{10}$$

where C_{cf} is a model constant. C_{cf} is calibrated to be 28.0 in a noisy environment and 45.0 in a quiet environment (the freestream turbulent intensity Tu_∞ is much less than 0.1%) based on the experimental data from HIFiRE-5 test cases. The function $F_{\text{ratio}}(Ma_{eL}, T_{eL}, T_w)$ is defined in Eq. (3). The crossflow strength term ΔH_{cf} is given by

$$\Delta H_{\text{cf}} = H_{\text{cf}} \left(1.0 + \min\left(\frac{\mu_t}{\mu}, 0.4\right)\right), \tag{11}$$

where H_{cf} is a dimensionless crossflow strength that can be defined from the local helicity

$$H_{\text{cf}} = \frac{dHe}{U}, \tag{12}$$

in which U is the local velocity magnitude, d is the distance to the nearest wall, and He is the local helicity, which is defined as

$$\boldsymbol{U} = \left(\frac{u}{\sqrt{u^2+v^2+w^2}}, \frac{v}{\sqrt{u^2+v^2+w^2}}, \frac{w}{\sqrt{u^2+v^2+w^2}} \right)$$

$$\boldsymbol{\Omega} = \left(\frac{\partial w}{\partial y} - \frac{\partial v}{\partial z}, \frac{\partial u}{\partial z} - \frac{\partial w}{\partial x}, \frac{\partial v}{\partial x} - \frac{\partial u}{\partial y} \right) \tag{13}$$

$$He = | \boldsymbol{U} \cdot \boldsymbol{\Omega} |,$$

where $\boldsymbol{U}$ and $\boldsymbol{\Omega}$ are the unit velocity vector and vorticity vector, respectively. The helicity, by definition, is the magnitude of the scalar product of the velocity and the vorticity and thus indicates the nonalignment of the velocity and vorticity vectors. Therefore, the helicity is maximized if the flow is rotating around the velocity vector. A nonzero helicity value indicates a three-dimensional flow.

Therefore, the transition onset function is defined as follows:

$$\begin{aligned}
&F_{\text{onset,s}} = \frac{Re_v}{F_{\text{ratio}}(Ma_{eL}, T_{eL}, T_w) Re_{\theta c}}, \quad F_{\text{onset,cf}} = \frac{\Delta H_{\text{cf}} Re_v}{F_{\text{ratio}}(Ma_{eL}, T_{eL}, T_w) C_{\text{cf}}} \\
&F_{\text{onset1}} = \max(F_{\text{onset,s}}, F_{\text{onset,cf}}) \\
&F_{\text{onset2}} = \min\left(\max\left(F_{\text{onset1}}, F_{\text{onset1}}^4 \right), 2.0 \right) \\
&F_{\text{onset3}} = \max\left(1 - \left(\frac{R_T}{2.5} \right)^3, 0 \right), \quad R_T = \frac{\rho k}{\mu \omega} \\
&F_{\text{onset}} = \max\left(F_{\text{onset2}} - F_{\text{onset3}}, 0 \right)
\end{aligned} \tag{14}$$

In addition, the original F_{length} function is formulated following the results of low-speed experiments. The transition momentum thickness Reynolds number of a hypersonic flow is usually large, which leads to the value of the original F_{length} becoming too small or even close to zero. This greatly affects the generation source term in the intermittency factor γ equation. Hence, the model function F_{length} is recalibrated to 20.0:

$$F_{\text{length}} = 20.0\left(1.0 - F_{\text{sublayer}}\right) + 40.0 \cdot F_{\text{sublayer}} \tag{15}$$

Finally, considering the accuracy in the prediction of the turbulent region hypersonic flows, the compressibility corrections are applied to k-ω SST turbulence model.

3. Model Validation

To validate the improved model, high-speed transition flows over flat plates, circular cones, Double Ramp, HIFiRE-5 and X-33 vehicles were simulated. The flow parameters are listed in Table 1.

Table 1. Flow conditions for the flat plate cases.

Case	Ma_∞	Re_∞/ m	T_∞, K	Tu_∞, %
Flat plate	6.1	4.9×10^6	800.0	0.32
Flat plate	6.2	2.6×10^6	690.0	0.32
straight cone	5.5	1.35×10^7	165.56	0.30
straight cone	5.5	9.19×10^6	161.67	0.30
straight cone	5.5	8.53×10^6	168.33	0.30
straight cone	5.5	6.56×10^6	146.11	0.30
straight cone	6.0	2.03×10^7	63.32	0.40

straight cone	6.0	1.77×10^7	63.32	0.40
HIFIRE-1	7.16	8.53×10^7	262.17	0.50
Double Ramp	8.1	3.8×10^6	106.0	0.50
HIFIRE-5	5.8	10.2×10^6	56.03	0.37
HIGIRE-5	5.8	8.1×10^6	56.03	0.37
HIGIRE-5	6.0	11.8×10^6	56.03	0.006
HIGIRE-5	6.0	10.2×10^6	56.03	0.006
X33 vehicle	6.0	2.59×10^7	62.10	0.10
X33 vehicle	6.0	1.97×10^7	62.10	0.10

In the first test case, a hypersonic boundary layer flow over a flat plate is analyzed to evaluate the effectiveness of the improved γ-Re_θ transition model. The plate length is 1500 mm and the flow conditions are consistent with the experimental study of Mee [12]. The wall temperature is T_w = 300 K. FIG. 1 shows comparisons of the computational Stanton numbers St with the experimental data under four different conditions. All the transition onset locations predicted by the improved transition model are consistent with the experimental data.

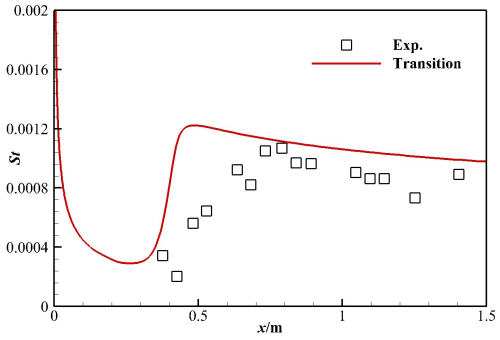

a) Ma_∞ = 6.1, Re_∞ = 4.9×10^6 /m.

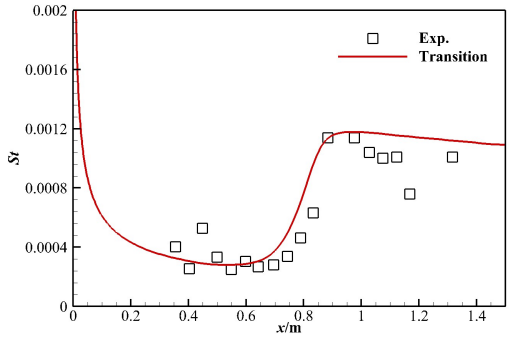

b) Ma_∞ = 6.2, Re_∞ = 2.6×10^6 /m.

FIG. 1 Predicted results for flat plate cases.

The cone has a half-cone angle of 8° at Ma_∞ = 5.5 [13]. Since the bluntness of the cone is not explicitly given in the experiment, 0.00254mm is used. The T_w =300 K. FIG. 2 presents the numerical results for the sharp cone at Mach 5.5. In FIG. 2, the centerline surface heat flux Q distributions are plotted vs the s which denotes the surface distance from the original nose tip. The vertical dashed lines are different Re_∞ experimental transition onsets. The results show good agreement with the experimental results. The next cone length is 636 mm, the nose bluntness is 0.00254 mm, and the half-cone angle is 5° [14]. The T_w =300 K. Comparisons with the present improved model at Mach 6.0 are shown in FIG. 3. With increasing Re_∞, the transition onset gradually moves forward. The overall variations computed from the present model are satisfactory. The Hypersonic International Flight Research Experimentation (HIFIRE-1) has a 7° half-cone-angle conical section, followed by a cylinder, a 33 deg flare, and a short flat cylindrical section with a 0.01 mm nose bluntness [15,16]. The T_w =294.78 K. FIG. 4 shows the flow features for the case. FIG. 5 presents the numerical results for the sharp case. The results show that the present model predicts the heat transfer and wall pressure distributions reasonably accurately. After the cone-cylinder juncture, both the heat flux and pressure sharply decrease and then noticeably increase in the flared section.

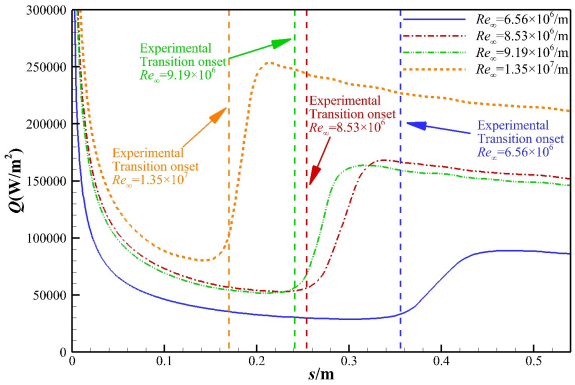

FIG. 2 Predicted results for the sharp cone cases at Ma_∞ = 5.5.

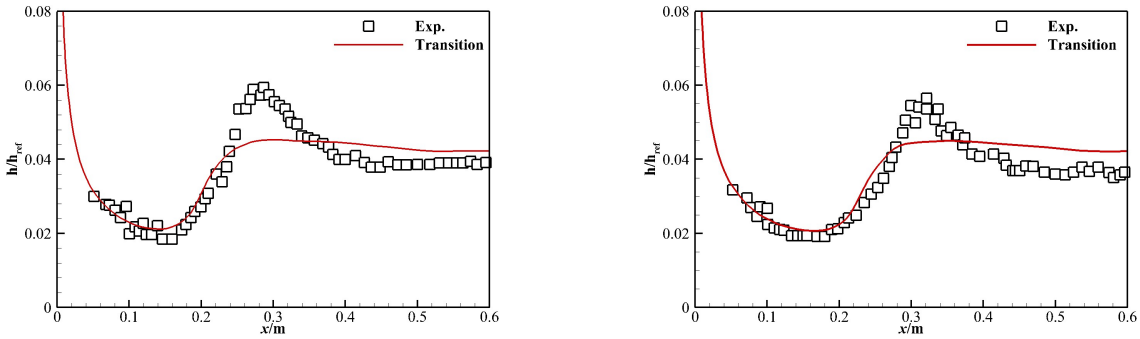

a) $Ma_\infty = 6.0$, $Re_\infty = 2.03 \times 10^7$ /m.

b) $Ma_\infty = 6.0$, $Re_\infty = 1.77 \times 10^7$ /m.

FIG. 3 Predicted results for sharp cone cases at Ma_∞ = 6.0.

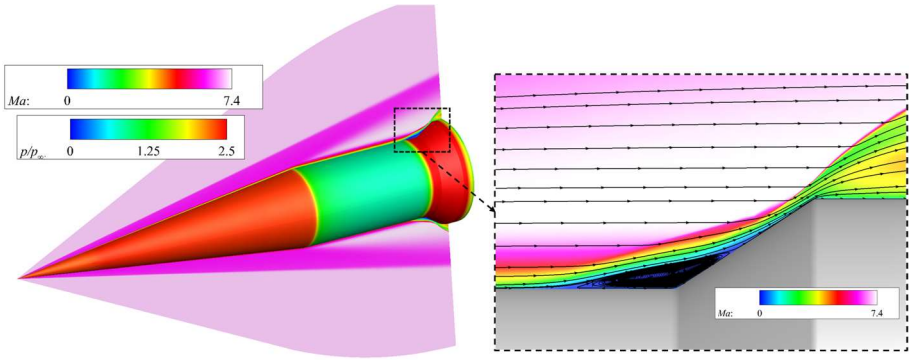

a) A symmetry cut plane of the Mach number and surface dimensionless pressure p/p_∞.

b) A local enlarged view of the Mach number contour at the cylinder-flare juncture.

FIG. 4 Flow features for the HIFIRE-1.

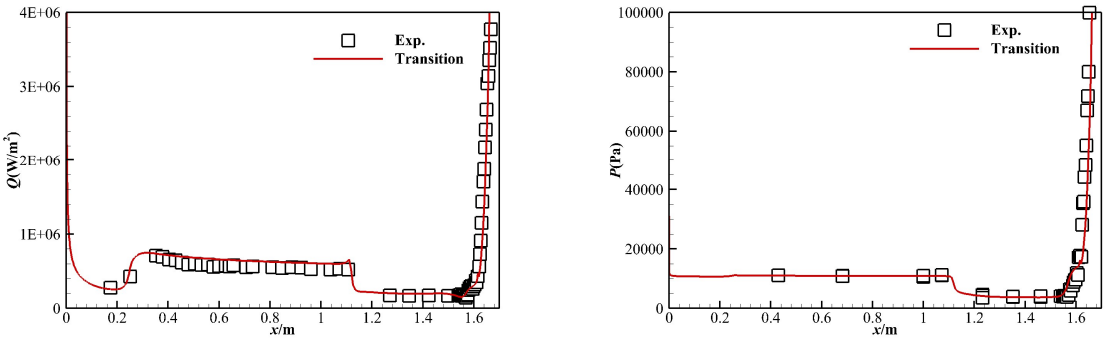

a) Wall heat flux distribution.

b) Wall pressure distribution.

FIG. 5 Predicted results for HIFIRE-1 at Mach 7.16.

The test case is a double ramp configuration with a sharp leading edge (Rn=0mm), as experimentally investigated by Neuenhahn and Olivier [17]. The first ramp is characterized by an angle of 9° and a length of 180 mm, and the second ramp features an angle of 20.5° and a length of 255 mm. FIG. 6 shows the numerical shadowgraph of the double ramp simulated by the improved γ-Re_θ transition model at T_w=300K. It can be seen that a strong leading shock occurs at the leading-edge region. Around the compression corner, separation occurs at the first ramp, followed by reattachment at the second ramp. The separation shock, separation bubble, and reattached shock are clearly discernible. The simulated flow structures are in good agreement with the features captured in the experimental schlieren image [17] presented in FIG. 7.

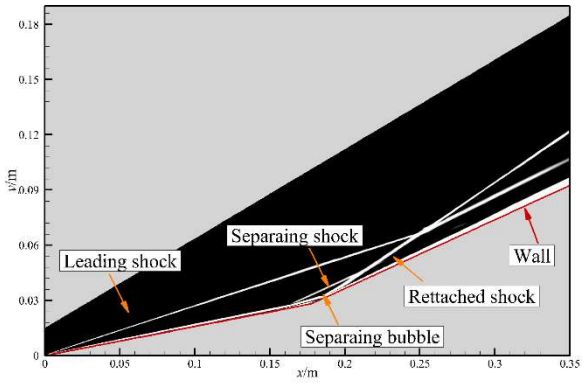

FIG. 6 Shadowgraph of double ramp simulated by the current model.

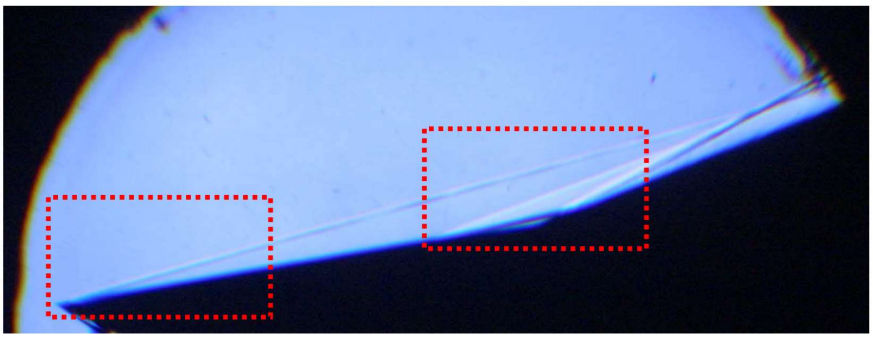

FIG. 7 Schlieren image of double ramp obtained from experiment.

The wall pressure coefficient Cp and Stanton number St distributions for the different T_w are shown in FIG. 8-FIG. 9. Both the laminar and transitional results for C_p agree well with the experimental data. The laminar and transitional results for the S_t distributions consistent with the experimental measurements in the laminar region on the first ramp and in the region around the separation bubble.

Because the transition occurs, the transitional result departs from the laminar solution and quickly increases to the turbulent level.

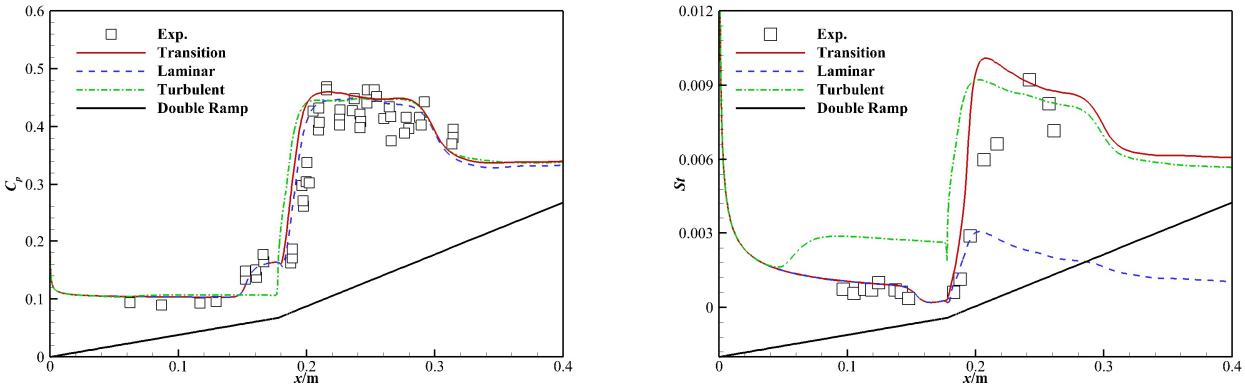

a) Wall C_p distribution. b) Wall St distribution.

FIG. 8 Predicted results for double ramp at T_w=300K.

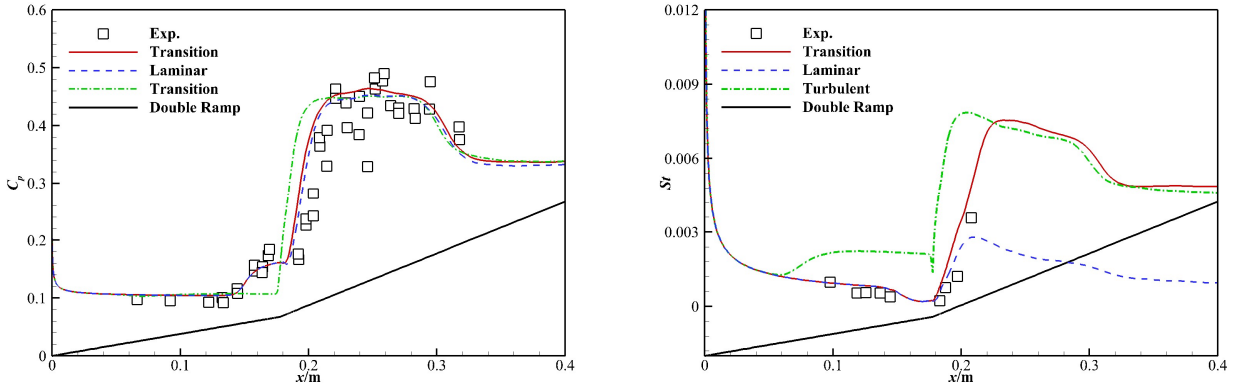

a) Wall C_p distribution. b) Wall St distribution.

FIG. 9 Predicted results for double ramp at T_w=600K.

The Hypersonic International Flight Research Experimentation (HIFiRE-5) is devoted to aerothermodynamic experiments and transitions in 3D geometries in particular. The HIFiRE-5 has a 7 deg half-angle on the minor axis, a 2.5-mm-radius nose tip, and a length of 0.86 m. The 38.1% scale model tested in the Boeing/Air Force Office of Scientific Research (AFOSR) Mach-6 Quiet Tunnel [18,19] is employed here to validate crossflow-induced transition. The general inflow conditions are α = 0° and T_w/T_0 = 0.7.

FIG. 10-FIG. 11 show the experimental TPS contour results and computational heat flux distributions at different Reynolds numbers. As shown by the experimental results, the transition onset is further behind in the quiet environment than in the noisy environment. As the Reynolds number Re_∞ increases, the transition onset moves forward. The prediction results successfully reflect the changes in the transition onset locations.

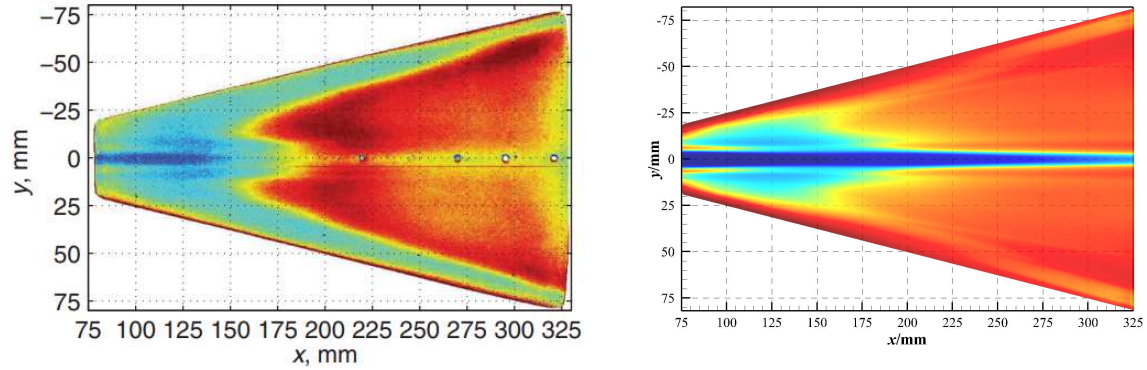

a) Experiment, TPS image, Re_∞ = 10.2 × 10^6 /m. b) Prediction, heat flux, Re_∞ = 10.2 × 10^6 /m.

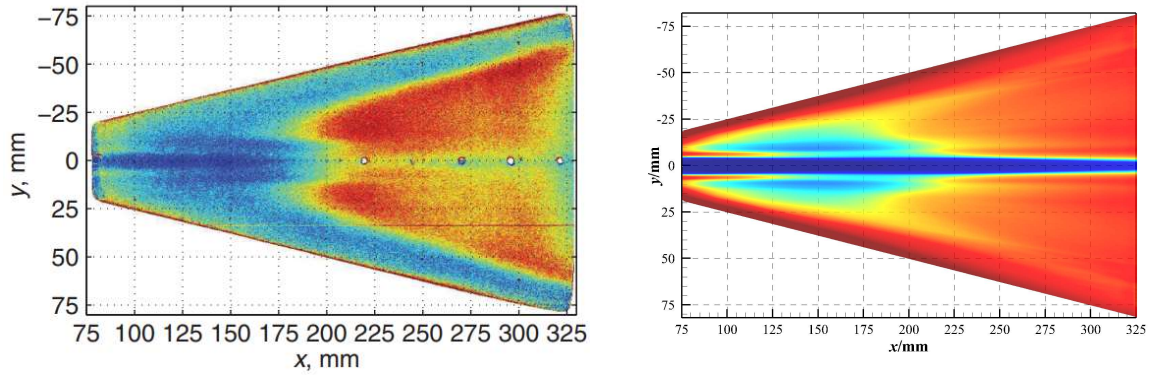

c) Experiment, TPS image, $Re_\infty = 8.1 \times 10^6$ /m. d) Prediction, heat flux, $Re_\infty = 8.1 \times 10^6$ /m.

FIG. 10 Predicted results for the HIFIRE-5 at Noisy flow.

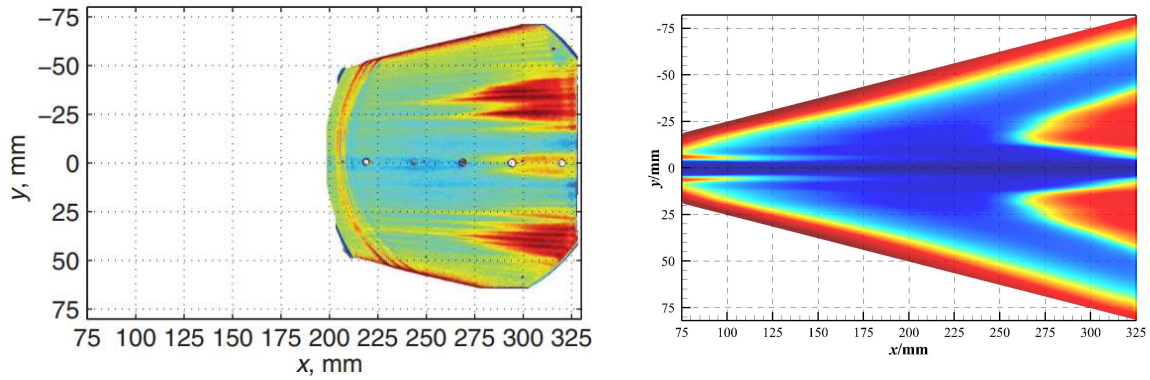

a) Experiment, TPS image, $Re_\infty = 11.8 \times 10^6$ /m. b) Prediction, heat flux, $Re_\infty = 11.8 \times 10^6$ /m.

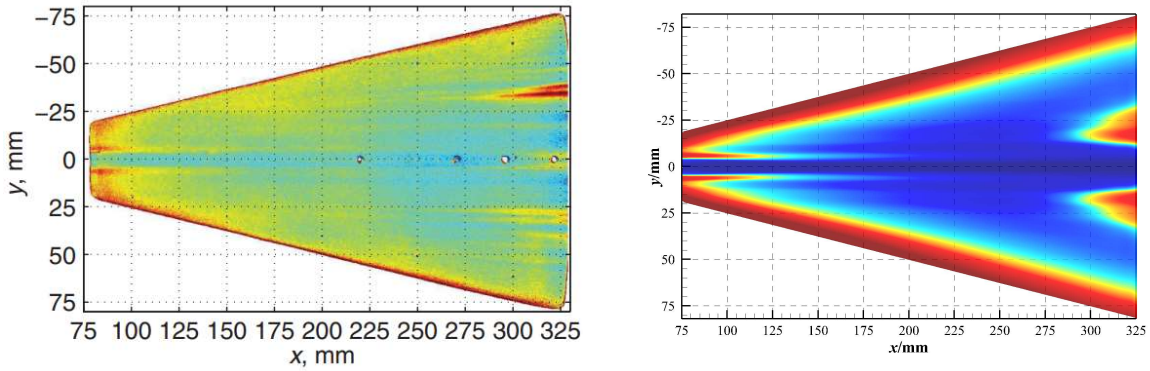

c) Experiment, TPS image, $Re_\infty = 10.2 \times 10^6$ /m. d) Prediction, heat flux, $Re_\infty = 10.2 \times 10^6$ /m.

FIG. 11 Predicted results for the HIFIRE-5 at Quiet flow.

The X-33 vehicle is selected in this section to test the improved γ-Re_θ transition model for the complex hypersonic configuration transition. The X-33 vehicle model is the same as the 0.0132-scale model in the NASA Langley Research Center (LaRC) 20-inch Mach 6 wind tunnel experiments of Berry et al. [20]. The length of the model is 25.4 cm, the maximum span across the canted fins is 30.62 cm, and the body-flap deflection is 20°. The wall temperature T_w is 300 K. The half-vehicle model is used in computations.

The typical flow structures around the X-33 vehicle are shown in FIG. 12. The Mach number Ma contours with streamlines on the symmetry plane are illustrated. The wall is colored based on the dimensionless pressure P/P_∞. The large attack angle and the large aircraft head generate a bow shock, which results in a low Mach number and high surface pressure. On the windward side of the aircraft, the bow shock is relatively close to the wall and the surface pressure increases. On the leeward side, the flow begins to expand and the surface pressure generally decreases. At the bottom of the aircraft, the flow further expands and the separation region appears. The flow structure is complex. The shock structure calculated in this paper is basically consistent with wind tunnel schlieren results. This shows

that the in-house solver used in this paper can capture such hypersonic complex flow structures highly accurately.

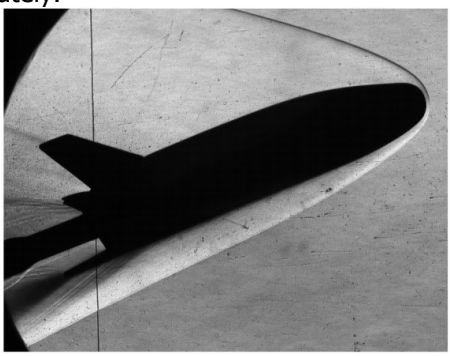

A) Wind tunnel schlieren image[21].

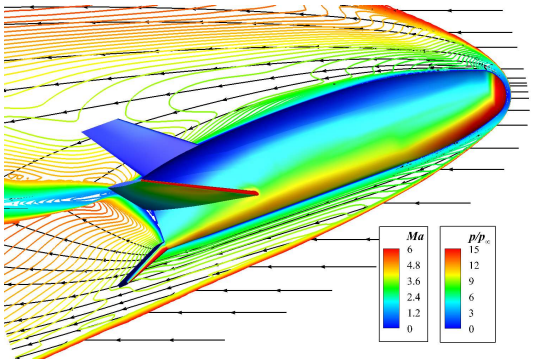

b) Streamline pattern distribution and contours of the Mach number and surface dimensionless pressure p/p_∞.

FIG. 12 Flow features for the X-33 model.

The heat transfer coefficient h/h_{ref} distributions computed using the improved γ-Re_θ model are compared with the experimental results at $Re_\infty = 2.59 \times 10^7$ /m in FIG. 13. On the windward side of the X-33 model, the transition zone predicted by the improved γ-Re_θ model occurs on both sides of the centerline, resulting in an M-shaped transition front. The computational result for the h/h_{ref} distribution from the improved γ-Re_θ model agrees well with the experiment result.

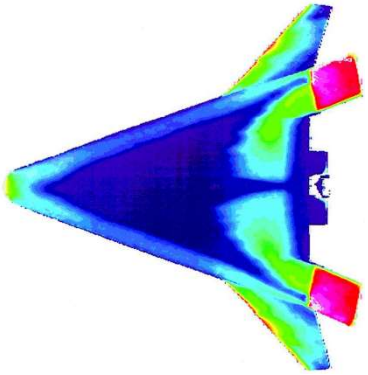

a) Experiment, h/h_{ref} distribution, $Re_\infty = 2.59 \times 10^7$ /m.

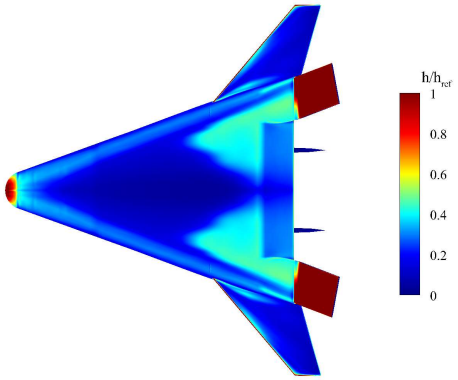

b) Prediction, h/h_{ref} distribution, $Re_\infty = 2.59 \times 10^7$ /m.

FIG. 13 Predicted results for the X-33 model.

FIG. 14 compares the centerline h/h_{ref} distributions on the windward side calculated using the improved γ-Re_θ model for different Reynolds numbers with the experimental wind tunnel results. It can be seen that the computational centerline h/h_{ref} distributions for different Reynolds numbers almost perfectly agree with the experimental wind tunnel data. Therefore, it can be concluded that the improved γ-Re_θ model allows the prediction of complex hypersonic configuration transitions.

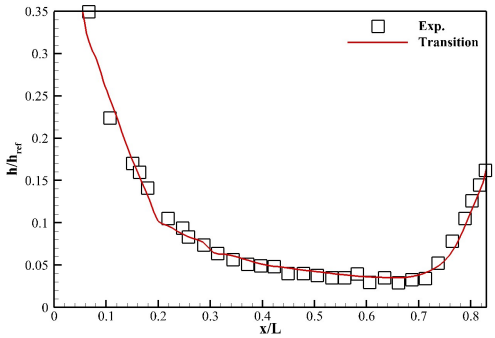

a) $Re_\infty = 2.59 \times 10^7$ /m.

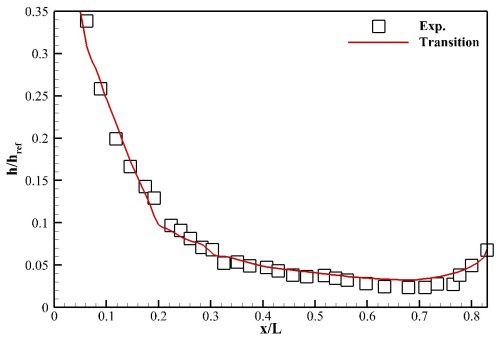

b) $Re_\infty = 1.97 \times 10^7$ /m.

FIG. 14 The X-33 model h/h_{ref} distribution along the centerline.

4. Conclusions

The numerical results showed that both the transition onset and the length of the transition region predicted by the improved γ-Re_θ transition model agree well with experimental data. In the HIFiRE-5 simulations, the influence of quiet and noisy flow conditions was considered. Meanwhile, the transition onset predicted by the improved γ-Re_θ transition model moved forward as the freestream Reynolds number increased, which indicates that the Reynolds number effects on the transition were also correctly predicted. The application of the improved γ-Re_θ transition model to an X-33 vehicle proved that this model allows the prediction of transitions on some complex full aircraft hypersonic configurations.

References

1. F. R. Menter, R. B. Langtry, S. R. Likki et al., "A correlation-based transition model using local variables—Part I: Model formulation," J. Turbomach. 128(3), 413-422 (2006) [DOI: 10.1115/1.2184352].
2. R. B. Langtry, F. R. Menter, S. R. Likki, Y. B. Suzen, P. G. Huang, and S. Völker, "A correlation-based transition model using local variables—Part II: Test cases and industrial applications," J. Turbomach. 128(3), 423-434 (2006) [DOI: 10.1115/1.2184353].
3. R. B. Langtry and F. R. Menter, "Correlation-based transition modeling for unstructured parallelized computational fluid dynamics codes," A.I.A.A. J. 47(12), 2894-2906 (2009) [DOI: 10.2514/1.42362].
4. D. C. Wilcox, "Turbulence-model transition predictions," A.I.A.A. J. 13(2), 241-243 (1975) [DOI: 10.2514/3.49679].
5. Z. Liu, Y. Lu, J. Li, C. Yan, "Local correlation-based transition model for high-speed flows," A.I.A.A. J. 60(3), 1365-1381 (2022) [DOI: 10.2514/1.J060994].
6. Z. Liu, Y. Lu, F. Xiao, C. Yan, "Further developments to a local correlation-based transition model for hypersonic flows," A.I.A.A. J. 60(6), 3909-3916 (2022) [DOI: 10.2514/1.J061585].
7. C. Li, Z. Gao, M. Zhao, C. Jiang, C. Lee, "Compressible modification of boundary-layer momentum thickness localized method in transition model," Int. J. Heat Fluid Flow 98, 109068 (2022) [DOI: 10.1016/j.ijheatfluidflow.2022.109068].
8. J. Xu, J. Bai, Z. Fu et al., "Parallel compatible transition closure model for high-speed transitional flow," A.I.A.A. J. 55(9), 3040-3050 (2017) [DOI: 10.2514/1.J055711].
9. L. Qiao, J. Xu, J. Bai, and Y. Zhang, "Fully local transition closure model for hypersonic boundary layers considering crossflow effects," A.I.A.A. J. 59(5), 1692-1706 (2021) [DOI: 10.2514/1.J059765].
10. R. Narasimha, "The laminar-turbulent transition zone in the boundary layer," Prog. Aerosp. Sci. 22(1), 29-80 (1985) [DOI: 10.1016/0376-0421(85)90004-1].
11. Z. Hao, C. Yan, L. Zhou, Y. Qin, "Development of a boundary layer parameters identification method for transition prediction with complex grids," Proc. Inst. Mech. Eng. G 231(11), 2068-2084 (2017) [DOI: 10.1177/0954410016660872].
12. D. J. Mee, "Boundary-layer transition measurements in hypervelocity flows in a shock tunnel," A.I.A.A. J. 40(8), 1542-1548 (2002) [DOI: 10.2514/2.1851].
13. G. H. Rushton and K. F. Stetson, "Shock tunnel investigation of boundary layer transition at M equals 5.5," A.I.A.A. J. 5, 899 (1967). [DOI: 10.2514/3.10166]

14. T. Horvath, S. Berry, B. Hollis, B. Singer, C. Chang, "Boundary layer transition on slender cones in conventional and low disturbance Mach 6 wind tunnels. 32nd AIAA fluid dynamics conference and exhibit." (2002), Vol. 2743 [DOI: 10.2514/6.2002-2743].
15. M. Holden, T. Wadhams, M. MacLean, E. Mundy, "Experimental studies of shock wave/turbulent boundary layer interaction in high Reynolds number supersonic and hypersonic flows to evaluate the performance of CFD codes. 40th fluid dynamics conference and exhibit." (2010), Vol. 4468 [DOI: 10.2514/6.2010-4468].
16. J. G. Marvin, J. L. Brown, and P. A. Gnoffo, "Experimental database with baseline CFD solutions: 2-D and axisymmetric hypersonic shock-wave/turbulent-boundary-layer interactions," NASA/TM-2013-216604. (2013).
17. T. Neuenhahn, H.Olivier. "Influence of the wall temperature and the entropy layer effects on double wedge shock boundary layer interactions, 14th AIAA/AHI space planes and hypersonic systems and technologies conference." 2006: 8136. [DOI: 10.2514/6.2006-8136].
18. T. J. Juliano and S. P. Schneider, "Instability and transition on the HIFiRE-5 in a Mach 6 quiet tunnel," (Purdue University Press, IN, 2010). [DOI: 10.2514/6.2010-5004]
19. T. J. Juliano, M. P. Borg, and S. P. Schneider, "Quiet tunnel measurements of HIFiRE-5 boundary-layer transition," A.I.A.A. J. 53(4), 832-846 (2015). [DOI: 10.2514/1.J053189]
20. S. A. Berry, T. J. Horvath, B. R. Hollis, R. A. Thompson, H. H. Hamilton, "X-33 hypersonic boundary-layer transition," J. Spacecraft Rockets 38(5), 646-657 (2001). [DOI:10.2514/2.3750]
21. B. R. Hollis, "X-33 computational aeroheating/aerodynamic predictions and comparisons with experimental data," (National Aeronautics and Space Administration, Langley Research Center, 2003).